

1 **Laser ablation-inductively coupled plasma-mass spectrometry imaging of white**
2 **and grey matter iron distribution in Alzheimer's disease frontal cortex**

3

4 *Dominic J. Hare^{ab*†}, Erika P. Raven^{cd†}, Blaine R. Roberts^b, Mirjana Bogeski^b, Stuart*
5 *D. Portbury^b, Catriona A. McLean^{ef}, Colin L. Masters^b, James R. Connor^{gh}, Ashley I.*
6 *Bush^b, Peter J. Crouchⁱ, and Philip A. Doble^{a**}*

7

8 *^a Elemental Bio-imaging Facility, University of Technology Sydney, Australia.*

9 *^b The Florey Institute of Neuroscience and Mental Health, The University of*
10 *Melbourne, Australia.*

11 *^c Center for Functional and Molecular Imaging, Georgetown University Medical*
12 *Center, United States of America*

13 *^d Advanced Magnetic Resonance Imaging Section, Laboratory of Functional and*
14 *Molecular Imaging, National Institute of Neurological Disorders and Stroke,*
15 *National Institutes of Health, United States of America*

16 *^e Department of Anatomical Pathology, Alfred Hospital, Australia*

17 *^f Department of Medicine, Central Clinical School, Monash University, Australia*

18 *^g Department of Neural and Behavioral Sciences, Penn State Hershey Medical*
19 *Center, United States of America*

20 *^h Department of Neurosurgery, Penn State Hershey Medical Center, United States of*
21 *America*

22 *ⁱ Department of Pathology, School of Biomedical Sciences, University of Melbourne,*
23 *Australia*

24

25 ** Correspondence to: Dominic J. Hare, University of Technology Sydney, PO Box*
26 *123, Broadway, New South Wales, 2007, Australia. Email. dominic.hare@uts.edu.au;*
27 *Ph. +61 3 9035 9549*

28 *** Correspondence to: Philip A. Doble, University of Technology Sydney, PO Box*
29 *123, Broadway, New South Wales, 2007, Australia. Email. philip.doble@uts.edu.au;*
30 *Ph. +61 2 9514 1792*

31

32 *† These authors contributed equally.*

33

1 **Abstract**

2

3 Iron deposition in the brain is a feature of normal aging, though in several
4 neurodegenerative disorders, including Alzheimer’s disease, the rate of iron
5 accumulation is more advanced than in age-matched controls. Using laser ablation-
6 inductively coupled plasma-mass spectrometry imaging we present here a pilot study
7 that quantitatively assessed the iron content of white and grey matter in paraffin-
8 embedded sections from the frontal cortex of Alzheimer’s and control subjects. Using
9 the phosphorus image as a confirmed proxy for the white/grey matter boundary, we
10 found that increased intrusion of iron into grey matter occurs in the Alzheimer’s brain
11 compared to controls, which may be indicative of either a loss of iron homeostasis in
12 this vulnerable brain region, or provide evidence of increased inflammatory processes
13 as a response to chronic neurodegeneration. We also observed a trend of increasing
14 iron within the white matter of the frontal cortex, potentially indicative of disrupted
15 iron metabolism preceding loss of myelin integrity. Considering the known potential
16 toxicity of excessive iron in the brain, our results provide supporting evidence for the
17 continuous development of novel magnetic resonance imaging approaches for
18 assessing white and grey matter iron accumulation in Alzheimer’s disease.

19

1 **Introduction**

2

3 Disrupted iron metabolism appears to be a pathological hallmark in the Alzheimer's
4 disease brain (Roberts et al., 2011). Numerous studies have identified abnormal
5 increases in the iron concentration within a range of affected brain regions (Belaidi
6 and Bush, 2015), including accumulation on the β -amyloid senile plaques that are
7 characteristic of AD (Lovell et al., 1998). While a 2011 meta-analysis suggested a
8 possible citation bias has overstated the significance of iron *elevation* (Schrag et al.,
9 2011), it should not be ignored that disrupted iron homeostasis without a measurable
10 increase still has the potential to promote oxidative stress through improper redox-
11 silencing of this highly reactive species. Changes in chemical properties of brain iron
12 have been observed dating back over half a century (Hallgren and Sourander, 1960),
13 and contemporary biotechnology has identified a range of genetic and metabolic
14 factor that support iron dyshomeostasis as playing an important role in AD pathology
15 (Crespo et al., 2014).

16

17 Important iron regulatory proteins, including ferritin and transferrin appear to be both
18 dysfunctional and abnormally distributed in the AD brain (Connor et al., 1992a;
19 Connor et al., 1995; Connor et al., 1992b), potentially contributing to the reactive
20 'labile iron pool' through mismanagement of normal metabolic pathways.

21 Neuroinflammation, where glial cells promote the deposition of iron, contributes to
22 elevated oxidative stress and mitochondrial dysfunction, and may also promote the
23 aggregation of the β -amyloid peptide and tau protein, forming the plaques and tangles
24 characteristic of the disease (Ong and Farooqui, 2005). Combined with the natural
25 accumulation of iron in the aging brain, endogenous response to elevated cortical iron
26 (such as heme oxygenase-1, which degrades heme and can release free, reactive
27 ferrous [Fe^{2+}] iron) may represent an important biochemical mechanism preceding
28 neuronal damage in AD (Ward et al., 2014).

29

30 *In vivo* imaging of the AD brain using magnetic resonance imaging (MRI) has
31 provided useful insight into both structural changes (Bartzokis et al., 2003) and iron
32 deposition (Bartzokis et al., 2000; Langkammer et al., 2014), using techniques such as
33 R_2 and R_2^* relaxometry (Langkammer et al., 2010) and phase imaging (Zhu et al.,
34 2009). However, differentiation between white and grey matter iron distribution in the

1 neocortex using MRI is challenging, as typical MRI approaches are not absolutely
2 quantitative, there are multiple contributions to tissue contrast (including myelin, iron
3 and CSF), and have a spatial resolution that precludes fine detail definition of brain
4 iron distribution at micrometer scales. Because of these many limitations, MR
5 imaging of brain iron has been largely constrained to deep brain nuclei, such as the
6 basal ganglia, which contain the highest iron content throughout the brain.

7
8 In this study we employed quantitative iron imaging by laser ablation-inductively
9 coupled plasma-mass spectrometry (LA-ICP-MS) to compare the distribution of iron
10 in white and grey matter regions of *post mortem* AD and healthy control (HC) frontal
11 cortex tissue which are primarily affected by AD pathology. LA-ICP-MS employs a
12 focused beam (typically in the ultra-violet range) that ablates particles from the tissue
13 sample surface, which are then carried to the ICP-MS and measured on the basis of
14 mass-to-charge (m/z) ratio (Hare et al., 2015). LA-ICP-MS is highly specific and
15 sensitive to iron, with detection limits well below the typical biological concentrations
16 found in neurological tissue (O'Reilly et al., 2014). With appropriate signal
17 normalization and periodic sampling of standards with comparable matrix
18 composition, LA-ICP-MS can provide absolute quantitative information at the low
19 micrometer scale (1-100+ μm) (Hare et al., 2012a; Miliszkiewicz et al., 2015). As an
20 element-specific detector, LA-ICP-MS also permits simultaneous detection of
21 multiple analytes and generation of hyperspectral images. We exploited this capability
22 here by using phosphorus distribution as a proxy for white and grey matter, which
23 was then applied to differentiating iron distribution in the two regions of frontal
24 cortex tissue from both AD and HC brains.

25
26 **Materials and methods:**

27
28 *Human brain samples*

29
30 Formalin fixed and paraffin embedded AD ($n = 4$) and HC ($n = 5$) cortical tissue from
31 the superior frontal gyrus was obtained from the Victorian Brain Bank Network at the
32 Florey Institute of Neuroscience and Mental Health. All procedures were conducted in
33 accordance with the Australian National Health and Medical Research Council's
34 National Statement on Ethical Conduct in Human Research (2007), the Victorian

1 Human Tissue Act (1982), the National Code of Ethical Autopsy Practice (2002) and
 2 the Victorian Government policies and practices in relation to *post mortem* tissue. All
 3 tissue samples were previously genotyped and confirmed as apolipoprotein E3/E3
 4 allele carriers (Rembach et al., 2013). Subject details are given in Tables 1 and 2.
 5 Previous studies have shown that formalin fixation may effect absolute iron
 6 concentrations (Hackett et al., 2011; Hare et al., 2014a), particularly during long-term
 7 (approx. 4 years) storage of brain tissue (Schrag et al., 2010). However, storage in
 8 formalin for shorter periods (<18 months) was shown to have no effect on brain iron
 9 levels (Gellein et al., 2007). Regardless, all samples underwent identical preparation
 10 methods (fixation of whole brain in 20% neutral buffered formalin for <6 weeks prior
 11 to neuropathological examination, excision of tissue blocks, paraffin infiltration and
 12 embedding) to ensure relative comparisons were valid.

13

14 **Table 1:** Subject age, sex and *post mortem* interval details. Neither age ($p = 0.2$;
 15 Student's two-tailed *t*-test) nor *post mortem* interval ($p = 0.3$) differed between
 16 groups.

17

	Alzheimer's disease	Healthy control
Age (years); range	74.2 ± 8.0 (n = 4); 34.1	85.4 ± 2.1 (n = 5); 9.2
Male (female)	4 (0)	4 (1)
Post mortem interval (hours)	47.9 ± 11.9	34.5 ± 5.7

18

19 **Table 2:** Age, post mortem interval, disease duration, cause of death and AD family
 20 history (where applicable).

21

Case	Age (years)	Post mortem interval (hours)	Disease duration	Cause of death	Family history
AD1	54.2	56.0	~ 4 years, 6 months (early onset at ~ 49 years)	Pulmonary thromboembolism; deep vein thrombosis	Mother AD onset in her 70s, grandmother also had AD
AD2	88.3	49.5	~ 4 years	Dementia	Not known
AD3	68.5	71.0	Unsure (never saw regular doctor); minimum 4 yrs from neuropathological examination	Acute septicaemia; dementia	Mother AD onset in her late 80s
AD4	85.8	15.0	Diagnosed 18 months prior to death, date of onset not known	Multiple myeloma; cerebral arteriosclerosis	No family history
HCI	82.7	48.0	n/a	Cardiac tamponade, haemopericardium,	

				ruptured acute posterolateral left; ventricular myocardial infarction; ischaemic coronary artery disease	
HC2	82.5	22.0	n/a	Acute myocardial infarction; ischaemic heart disease; hypertension	
HC3	84.8	39.5	n/a	Acute myocardial infarction	
HC4	91.7	28.5	n/a	Complications of surgical correction of fractured neck of femur; general debility; hepatic abscess; ischaemic heart disease; chronic renal failure	
HC5	Unknown	Unknown	n/a	Ischaemic heart disease	

1

2

3 *Sample preparation for LA-ICP-MS*

4

5 Sections were cut on a standard microtome at 5- μ m thickness using
6 polytetrafluoroethylene-coated disposable blades (C.L. Sturkey, ProSciTech, Qld,
7 Australia) and mounted on silane-coated soda-glass microscope slides (StarFrost®;
8 ProSciTech). Sections were dewaxed in xylene (Merk Millipore, NSW, Australia) and
9 decreasing concentrations of ethanol (Merk Millipore) in water according to standard
10 protocols. Samples were finally washed in MilliQ water (18.2 M Ω ; Merk Millipore)
11 and dried at room temperature before analysis.

12

13 *LA-ICP-MS analysis*

14

15 Quantitative imaging of iron was performed using a NewWave NWR213 laser
16 ablation system (ESI Ltd., Bozeman, MT, USA) hyphenated to an Agilent
17 Technologies 8800 Series triple quadrupole ICP-MS (Mulgrave, VIC, Australia)
18 operating in single quadrupole acquisition mode with 3 mL min⁻¹ hydrogen reaction
19 gas to minimize polyatomic interference from ⁴⁰Ar¹⁶O⁺ on ⁵⁶Fe⁺ (Lear et al., 2012).
20 The NWR213 was fitted with a standard two-volume cell with a 10 cm x 10 cm

1 scanning area. Standard operating parameters for this system were used as previously
2 reported (Bishop et al., 2015). Mass-to-charge (m/z) ratios for carbon (13),
3 phosphorus (31) and iron (56) were acquired. Samples were ablated using a square 80
4 x 80 μm laser beam, producing pixels representing a total area of 6.4 mm^2 with a laser
5 energy fluence of approximately 1 J cm^{-2} , which was sufficient to ablate tissue but not
6 the underlying slide matrix. Signal noise accounted for approximately 0.3% of the
7 mean signal intensity for each section, and was thus considered negligible.
8 Phosphorus and iron data was normalized to the corresponding carbon-13 signal (see
9 Supplementary Fig. S1 for individual carbon-13 maps) recorded to compensate for
10 variation in laser power and sample transport effects (Austin et al., 2011). Iron images
11 were quantitated against representative ablation (carbon-13 normalized) of matrix-
12 matched tissue standards produced using metal-spiked homogenates of sheep cortical
13 brain tissue cut to an equivalent thickness on a cryostat (Hare et al., 2013b). Wet
14 weight concentrations are derived from the independent analysis of metal
15 concentrations in the standard reference materials and use the assumption that brain
16 water content is around 80% (Keep et al., 2012) for both the standards and sample
17 tissue sections. Four repeated five-point calibrations were recorded during the
18 experiment, with good linearity ($r^2 = 0.9485$) and reproducibility ($p = 0.4677$; $F =$
19 0.909 ; Supplementary Fig. S2). Images were produced using ENVI 5.3 (Exelis,
20 Boulder, CO, USA), background (scanned areas not containing tissue) pixels were
21 excluded using a carbon-13 mask, and regions of interest (ROIs) were extracted using
22 both ENVI 5.3 and Fiji (<http://fiji.sc/Fiji>, (Schindelin et al., 2012)). Statistical analysis
23 of extracted ROIs was performed using Prism 6.0e (GraphPad, La Jolla, CA, USA).
24 All comparisons were unpaired Student's two-tailed t -tests, with statistical
25 significance defined as $p < 0.05$. All data is reported as \pm standard deviation.

26 27 *Perls staining*

28
29 Adjacent 5- μm thick sections mounted on microscope slides were dewaxed as above,
30 and then extensively rinsed in running water. Hydrated sections were incubated at 37
31 $^{\circ}\text{C}$ for 1 hour in potassium ferrocyanide (7% w/v) in hydrochloric acid (3% v/v) and
32 then enhanced using a solution of 3.5 μM 3,3'-diaminobenzidine (DAB) in hydrogen
33 peroxide (0.015% v/v) for 5 minutes. After quenching the reaction by immersing in
34 running water, samples were counterstained with hematoxylin for 2 minutes and

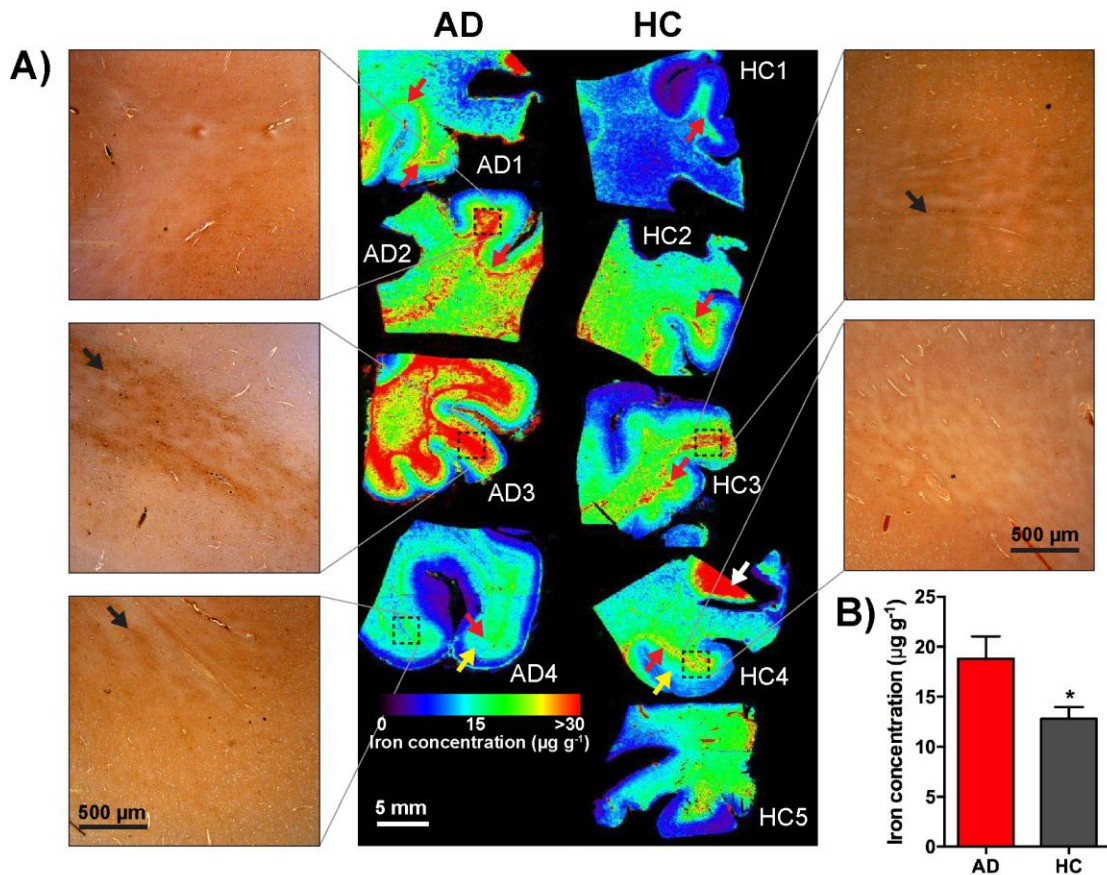
1 washed in water before dehydration in increasing ethanol concentration, xylene and
2 coverslipping. Micrographs were recorded using a Leica DM2500 optical microscope
3 with a 2.5×/0.50 NA lens and Leica DFC310FX digital camera.

5 *Myelin staining*

7 Myelin was histologically stained on additional adjacent 5- μ m thick sections using the
8 Luxol Fast Blue method. Sections were dewaxed and stained in 0.1% (w/v) Luxol
9 Fast Blue in methanol with 0.05% (v/v) acetic acid for 1 hour. White and grey matter
10 was differentiated in 0.05% (w/v) lithium carbonate for approximately 4 minutes.
11 Sections were then counterstained with Cresyl Violet for 1 hour, dehydrated, cleared
12 in xylene and coverslipped. Micrographs were recorded using the same equipment as
13 described above.

15 **Results:**

17 Quantitative images of iron in the AD and HC sections are presented in Fig. 1a
18 (shown here on the same scale, see Supplementary Fig. S3 for individually scaled
19 images). In AD tissue, mean iron concentration in the entire scanned section was
20 elevated compared to controls (mean iron concentration AD = $18.80 \pm 2.23 \mu\text{g g}^{-1}$;
21 HC = $12.80 \pm 1.17 \mu\text{g g}^{-1}$; $p < 0.05$, Student's two-tailed t -test; Fig. 1b). Perls staining
22 with DAB enhancement (Fig. 1a) revealed only minor non-heme iron deposition
23 within white matter. Iron could be associated with three specific distribution patterns
24 in both AD and HC tissue in each LA-ICP-MS image related to both grey and white
25 matter myelin content: i) cortical 'bands' of tangentially oriented, myelinated fiber
26 tracts (*e.g.* Bands of Baillarger), consistent with layer-specific MR contrast variations
27 attributed to the co-localization of these myelin bands with iron (Fukunaga et al.,
28 2010); ii) subcortical U-fibers found directly adjacent to the white-grey matter
29 boundary (Drayer et al., 1986); and iii) non-homogenous pattern in subcortical white
30 matter in the form of a diffuse, patchwork distribution previously reported using
31 immunohistochemistry by Connor and Menzies (Connor and Menzies, 1995) and in
32 subsequent mouse studies using LA-ICP-MS (Hare et al., 2014b).



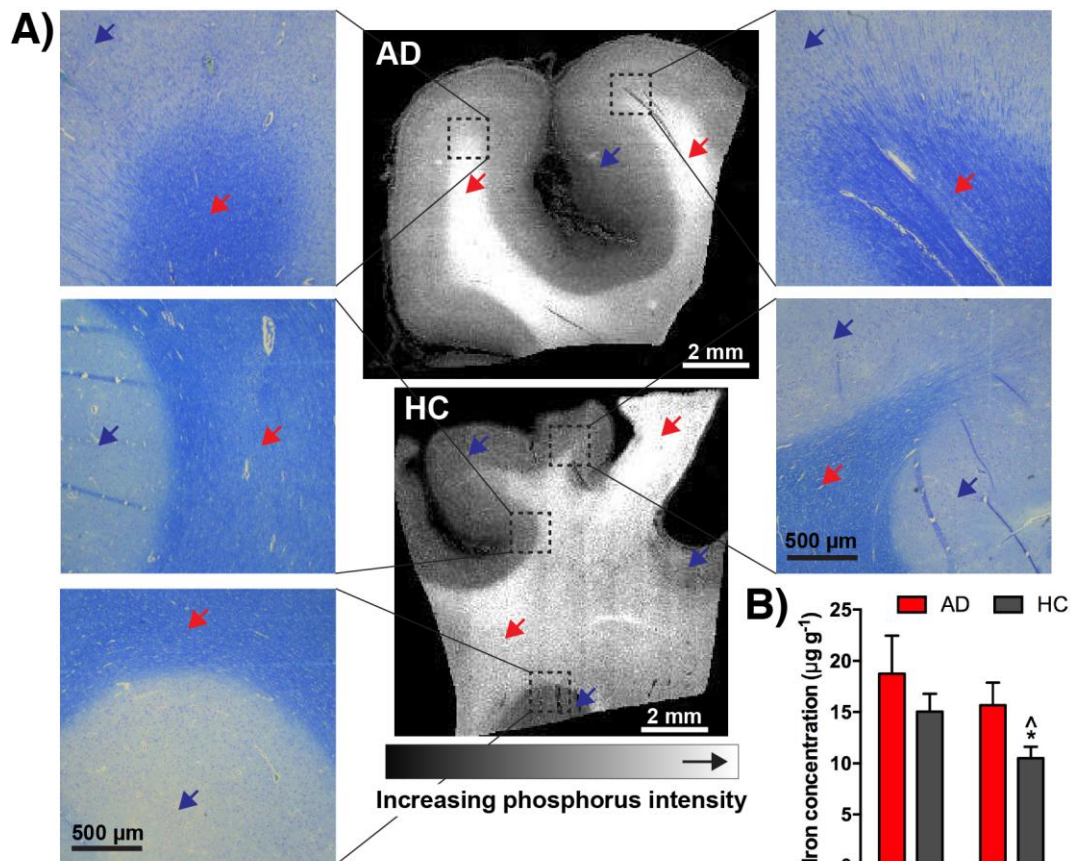
1

2 **Fig. 1.** A) Quantitative LA-ICP-MS imaging of iron levels in AD and HC frontal
 3 cortex sections (dewaxed paraffin-embedded) and corresponding Perls images from
 4 selected regions of interest in all samples analyzed. Perls staining with DAB
 5 enhancement revealed only minor intracellular increases in iron content visible within
 6 the white matter of AD brains, mirroring the ‘streaking’ pattern within these regions
 7 observed in LA-ICP-MS images, which was less obvious in age-matched HCs. Red
 8 arrows indicate subcortical iron; yellow arrows indicate cortical iron (see
 9 Supplementary Fig. S3); and black arrows showing corresponding areas in Perls
 10 stained sections. B) The combined white and grey matter iron levels in frontal cortex
 11 were significantly increased (*; $p < 0.05$; Student’s two-tailed t -test) in the AD
 12 sections. Error bars = 1 standard deviation between samples. Note: the white arrow
 13 indicates iron-rich caudate nucleus in one section, which was confirmed by Luxol
 14 Fast Blue staining and was excluded from the analysis.

15

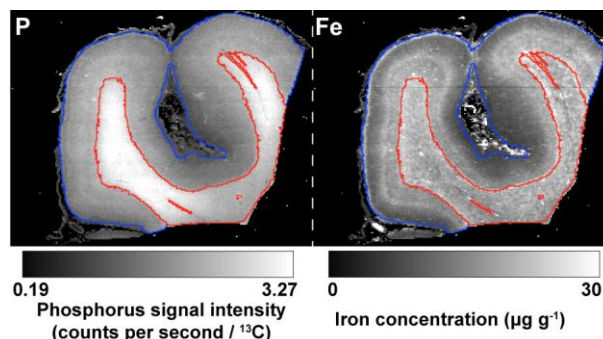
16 To demarcate the white-grey matter boundary, we used images of phosphorus (Fig.
 17 2a; Supplementary Fig. S4), which has been shown to effectively depict spatial
 18 myelin distribution using micro particle induced X-ray emission spectroscopy
 19 (μPIXE) with myelin immunostaining as a confirmatory comparator (Stüber et al.,
 20 2014), and is more concentrated in white matter (Duyn et al., 2007). LA-ICP-MS
 21 imaging is hyperspectral, where iron and phosphorus signal corresponds between
 22 pixels. A white matter mask was produced by a threshold function using bimodal
 23 distribution of phosphorus pixels. A grey matter mask was then produced using the

1 remaining pixels with the white matter values excluded. This mask was then applied
2 to iron images (Fig. 3). We confirmed that phosphorus imaging by LA-ICP-MS also
3 delineated white and grey matter with Luxol Fast Blue staining of myelin (Fig. 2a).
4 There was no apparent difference in relative phosphorus distribution between AD and
5 HC groups ($WM_{AD} = 2.53 \pm 0.49$, $WM_{HC} = 2.53 \pm 0.10$, $p = 1.0$; $GM_{AD} = 1.50 \pm 0.27$,
6 $GM_{HC} = 1.55 \pm 0.13$; $p = 0.7$; all units carbon-13 normalized phosphorus signal
7 intensity; Supplementary Fig. S5); and the ratio of white to grey matter volume
8 measured from the entire tissue section did not significantly differ according to
9 diagnostic group ($AD = 1.28 \pm 0.86$, $HC = 1.58 \pm 0.95$; $p = 0.63$; Supplementary Fig.
10 S6). Iron was present at a lower concentration in grey matter of the HC frontal cortex
11 ($WM_{HC} = 15.1 \pm 3.9 \mu\text{g g}^{-1}$; $GM_{HC} = 10.5 \pm 2.5 \mu\text{g g}^{-1}$; $p < 0.05$; iron concentrations
12 for each section are shown in Table 3), though in corresponding AD sections the
13 delineation of iron distribution within white and grey matter was lost ($WM_{AD} = 18.7 \pm$
14 $7.3 \mu\text{g g}^{-1}$; $GM_{AD} = 15.7 \pm 4.4 \mu\text{g g}^{-1}$; $p = 0.7$), which may be due to high variability
15 and the small sample size. Comparing white and grey matter between AD and HC
16 tissue, we found that iron was significantly elevated in the grey matter of AD brains
17 (+49%; $p < 0.05$), and showed a generalized, non-significant increasing trend in white
18 matter (+25%; $p = 0.4$; Fig. 2b). There was no significant difference in the grey matter
19 volume (determined as total area scanned from the phosphorus masks) between AD
20 and HC ($AD = 85.2 \pm 22.6 \text{ mm}^2$, $HC = 89.4 \pm 32.24 \text{ mm}^2$; $p = 0.83$; Supplementary
21 Fig. S7). It is unclear as to why errors associated with iron in AD tissue were
22 generally larger than HC samples, though we have observed that cellular iron
23 dyshomeostasis, such as is thought to be involved in AD pathology, demonstrates a
24 more variable concentration of iron, indicative of a system in crisis (James et al.,
25 2016).
26



1
2
3
4
5
6
7
8
9
10
11
12

Fig. 2. A) Myelin staining of sections from the same tissue block using the Luxol Fast Blue method confirms phosphorus imaging by LA-ICP-MS differentiates white (red arrows) and grey matter (blue arrows). B) Using the phosphorus images to delineate the white/grey matter boundary and simultaneously obtained iron LA-ICP-MS images, iron levels were quantified according to white/grey matter distribution. Iron levels in white matter did not differ significantly between experimental groups, though iron was significantly increased in the grey matter of the AD frontal cortex (*; $p < 0.05$; Student's two-tailed t -test). Also, the significant difference between white and grey matter in healthy controls (^; $p < 0.05$) was not observed in AD tissue sections ($p = 0.5$).



13
14
15
16
17
18

Fig. 3: Masks were generated using high (white matter; red line) and low phosphorus signal intensity values, which were then applied to quantitative iron images to extract white and grey matter regions of interest. Note excluded areas correspond to microscopic tears in the tissue section.

Table 3: Individual iron concentrations (± 1 standard deviation) and total measured area in the white matter, grey matter and the entire section (white and grey matter combined) for AD and HC sections analysed.

Case	White matter		Grey matter		Combined white and grey matter	
	Iron ($\mu\text{g g}^{-1}$)	Area (mm^2)	Iron ($\mu\text{g g}^{-1}$)	Area (mm^2)	Iron ($\mu\text{g g}^{-1}$)	Area (mm^2)
<i>AD1</i>	13.8 ± 5.2	44.3	15.6 ± 7.2	105.9	15.0 ± 13.2	150.2
<i>AD2</i>	19.5 ± 4.7	69.3	17.1 ± 6.3	101.9	19.1 ± 12.1	171.2
<i>AD3</i>	28.9 ± 10.8	94.2	20.2 ± 8.7	74.3	23.5 ± 18.9	168.5
<i>AD4</i>	12.8 ± 2.8	129.8	9.8 ± 3.6	58.6	10.6 ± 4.4	188.4
<i>HC1</i>	9.0 ± 3.0	55.2	7.2 ± 4.1	124.9	8.4 ± 4.9	180.1
<i>HC2</i>	16.4 ± 4.8	41.6	13.4 ± 7.9	114.1	15.3 ± 6.8	155.7
<i>HC3</i>	19.5 ± 5.1	130.3	12.0 ± 5.0	43.0	13.8 ± 7.0	173.3
<i>HC4</i>	14.3 ± 3.8	67.8	11.0 ± 4.0	78.2	13.0 ± 4.1	146.1
<i>HC5</i>	16.1 ± 9.3	61.6	9.0 ± 10.0	86.7	13.3 ± 10.3	148.3

Age is factor that is known to influence brain iron levels, particularly in the deep brain structures of the basal ganglia (Ward et al., 2014; Zecca et al., 2004), though there is some contention as to whether age-related changes occur in the frontal cortex. Ramos *et al.* (Ramos et al., 2014) and Bilgic *et al.* (Bilgic et al., 2012) found no evidence of elevated frontal cortex iron with respect to age, and that observed by Hebbrecht *et al.* (Hebbrecht et al., 1999) was comparatively very small *versus* the basal ganglia. Using a standard power calculation for type I error (Snedecor and Cochran, 1986), our sample size can detect a difference of $5.3 \mu\text{g g}^{-1}$, which is less than the observed difference in means of combined GM and WM in iron in HC and AD groups of $6.0 \pm 2.4 \mu\text{g g}^{-1}$ ($\alpha = 0.05$; power = 0.8).

Discussion

Considerations for post mortem artefact

Previously reported iron levels in digests of formalin-fixed frontal white matter, measured using solution nebulization ICP-MS, were markedly higher than our results; iron concentrations were $\sim 50\%$ of those reported in fixed frontal lobe tissue reported by others (Hallgren and Sourander, 1960; Langkammer et al., 2012a; Langkammer et al., 2012b). However, leaching did not appear to be specific to cortical tissue; the iron concentration in the caudate nucleus excluded from our analysis ($33.0 \pm 10.9 \mu\text{g g}^{-1}$)

1 showed a similar degree of iron loss compared to fixed but non-embedded tissue
2 (Langkammer et al., 2012b). To our knowledge, the effects of paraffin embedding and
3 deparaffinization on brain iron levels has not been reported, though a study comparing
4 fresh liver tissue to paraffin infiltrated and dewaxed samples showed a linear
5 relationship between iron concentrations *in lieu* of absolute quantitative
6 reproducibility (Beilby et al., 1999). Regardless, and as stated in the Materials and
7 Methods, all samples underwent identical preparation steps to ensure valid
8 comparisons. While it is possible that an altered chemical environment with respect to
9 iron in AD tissue is more susceptible to *post mortem* artefact, such as leaching during
10 the fixation and embedding process, the hypothesis that neurotoxicity in AD is related
11 to an increased labile iron pool (*i.e.* Fe²⁺) (Peters et al., 2015) is supported by our
12 data, which shows elevated iron levels are preserved in AD tissue even after extensive
13 chemical treatment. However, direct assessment of iron oxidation state is not practical
14 for archived tissue sections nor this analytical approach; fresh unfixed tissue and
15 species-specific imaging such as X-ray absorption near-edge structure (XANES)
16 spectroscopy would be required for this task (James et al., 2016). This pilot study is
17 justification for a similar validation experiment to those performed by Langkammer
18 and colleagues to categorically confirm association between QSM and *post mortem*
19 iron levels (Langkammer et al., 2010; Langkammer et al., 2012b), where in this case
20 the effects of paraffin embedding, which clearly results in a uniform loss of iron from
21 neurological tissue, are characterized and defined. Doing so would make available
22 decades' worth of archived samples for metal analysis.

23

24 *White/grey matter iron ratios*

25

26 Subcortical white matter contains some of the lowest concentration of iron within the
27 brain (Krebs et al., 2014; Riederer et al., 1989), particularly compared to the basal
28 ganglia (Hare et al., 2012b; Zecca et al., 1994). Corresponding cortical grey matter
29 also contains comparatively less non-heme iron (Hallgren and Sourander, 1960). Our
30 results from age-matched healthy controls show that cortical grey matter contains less
31 *total* iron than adjacent white matter. These data are in agreement with historical
32 values; (Hallgren and Sourander, 1958) reported that the ratio of iron in frontal white
33 matter to prefrontal cortex was 1.45, and we observed a similar ratio of 1.43 in
34 healthy controls.

1

2 *Relevance to MRI imaging of brain iron*

3

4 Myelin is known to introduce significant bias in magnetic susceptibility MRI
5 (Lodygensky et al., 2012), with this bias strongest in myelin-rich white matter. Field
6 dependent relaxation rate increase (FDRI) MRI is more robust to ferritin iron content,
7 although is susceptible to registration error between scanning sessions (Daugherty and
8 Raz, 2015). Thus, *in vivo* assessment of iron accumulation is often most suited to
9 diseases affecting areas of natively high iron and low myelin content, such as the
10 basal ganglia in Parkinson's disease (Rossi et al., 2013). In this study, the use of
11 phosphorus as a proxy for myelin, which has previously been described using
12 alternative microchemical imaging methods (Stüber et al., 2014), was further
13 confirmed as a suitable means for differentiating myelin from iron using hyperspectral
14 imaging and defining the white/grey matter boundary. Though it is only of practical
15 use in *post mortem* studies, it may assist in the further development of new MRI
16 approaches for discerning between these two interfering factors.

17

18 *Iron reactivity, aging and Alzheimer's disease pathology*

19

20 Although iron concentrations in cerebral white matter are difficult to quantitatively
21 assess by MRI due to both interferences from myelin and heterogeneous iron
22 distributions, the latter point should not be taken as it having an insignificant role in
23 brain aging and age-related disorders like AD. Numerous histological and MRI
24 studies have identified significant age-related changes first appearing in the cerebral
25 white matter (Gunning-Dixon et al., 2009). For example, R_1 with diffusion MRI of
26 white matter measured over a large cohort spanning 80 years identified a slow decline
27 beginning at 40+ years of age (Yeatman et al., 2014). More sensitive techniques such
28 as LA-ICP-MS, which are capable of measuring small changes in iron levels at a high
29 spatial resolution are therefore an important tool in understanding the role of iron in
30 disease pathogenesis. Central to the brain iron deposition and free radical theory of
31 aging is that a loss of iron homeostasis results in the accumulation of reactive iron(II),
32 which mediates the generation of harmful reactive oxygen species (ROS) (Schipper,
33 2004). This occurrence may not necessarily result in a measure of accumulation of
34 iron. Rather, the redistribution of iron from safe storage in proteins like ferritin to the

1 cytoplasm may be sufficient to initiate a cascading Fenton reaction, where iron
2 repeatedly cycles through the ferrous and ferric oxidation states to produce a constant
3 source of free radicals that eventually overwhelm endogenous antioxidant
4 mechanisms (Hare et al., 2013a). Therefore, lower iron levels in white matter
5 compared to the deep brain structures of the basal ganglia should not be viewed as an
6 insignificant contributor to either normal brain aging, or age-related
7 neurodegeneration, such as AD. White matter is particularly lipid-rich, and thus
8 highly susceptible to peroxidation and loss of cellular and structural integrity in AD
9 (Bartzokis et al., 2003) *via* iron-catalyzed free radical generation.

10
11 Although a causal relationship between increased iron reactivity and AD has not been
12 categorically confirmed, there is mounting evidence that it plays an important
13 upstream role in cell death. For instance, the recently-described non-apoptotic form of
14 cell death termed ‘ferroptosis’ (Dixon et al., 2012) induces necrosis via iron-mediated
15 production of ROS and has been implicated in motor neuron degeneration (Chen et
16 al., 2015). The generalized increase in cortical grey matter iron observed in our pilot
17 study lends further support to iron playing a critical role in neurodegeneration within
18 the AD brain. Disrupted iron metabolism, such as impaired activity of the amyloid
19 precursor protein (Duce et al., 2010), which is essential to the stabilization of the
20 membrane-bound iron export protein ferroportin (Wong et al., 2014), can lead to an
21 increase in the labile iron pool within neurons, facilitating increased ROS generation.
22 When combined with R_2 relaxometry, FDRI MRI has shown a relationship between
23 iron accumulation in ferritin and loss of tissue integrity in the hippocampus of AD
24 patients (Raven et al., 2013). Iron has also been associated with accumulation around
25 extracellular amyloid plaques in humans (Connor et al., 1992a; Lovell et al., 1998).
26 Our LA-ICP-MS technique likely lacks the resolution to discern these microscopic
27 structures (Lovell et al.’s study used micro-particle induced X-ray emission
28 spectroscopy with a per-pixel resolution of $50 \mu\text{m}^2$), though a study using X-ray
29 fluorescence microscopy with a similar resolving power ($60 \mu\text{m}^2$) found elevated
30 extracellular iron in the PSAPP mouse model of AD that displays similar plaque
31 pathology was *not* associated with the β -amyloid inclusions (Leskovjan et al., 2011).
32
33 Increased iron in the grey matter may indicate either a loss of iron homeostasis, or a
34 brain region at higher risk of iron-mediated neurodegeneration. Previous studies of

1 iron regulatory proteins in cortical tissue found a generalized decrease in transferrin
2 levels in grey matter and consistent distribution of ferritin (Connor et al., 1992b). This
3 may be indicative of a higher degree of ferritin saturation as a compensatory
4 mechanism for increased grey matter iron, though Perls staining did not reveal an
5 observable amount of increased non-heme iron within this region. Another possible
6 scenario reflective of increased grey matter iron is the inflammatory process
7 underway within the degenerating region. *In vitro* studies of astrocytes and microglia
8 cultured from *post mortem* AD white and grey matter has shown grey matter-sourced
9 cells proliferate more rapidly than white matter counterparts (Blasko et al., 2004). Our
10 hypothesis is supported by a recent study using high field 7 Tesla MRI and
11 histological assessment (*via* the same Perls-DAB method employed here) of *post*
12 *mortem* AD tissue, which showed correlation between grey matter iron and activated
13 microglia in AD, as well as a similar staining within white matter (Zeineh et al.,
14 2015). This pattern of non-heme iron is consistent with elevated levels of ferritin
15 within white matter (Fukunaga et al., 2010; van Duijn et al., 2013), and the more
16 prominent Perls staining in AD tissue may also be reflective of the pathological
17 accumulation of this iron storage protein previously observed in the hippocampus
18 (Raven et al., 2013), preceding a loss of structural integrity in the frontal cortex white
19 matter occurring later in the disease. Chronic inflammation is a cardinal feature of AD
20 (Gomez-Nicola and Boche, 2015) and neurodegeneration in general (De Lucia et al.,
21 2015), and targeting inflammatory pathways and microglial activation is a promising
22 avenue for therapeutic development (Olmos-Alonso et al., 2016). Our observed
23 increase in iron levels within the degenerating grey matter supports that this region is
24 under duress and initiates a response mechanism highly dependent on iron-mediated
25 enzymatic processes, which in turn has a follow-on effect on oligodendrocyte health
26 and myelin integrity in white matter. Further, hypometabolism (which is associated
27 with iron deposition and white matter damage in the aceruloplasmenic brain
28 (Miyajima et al., 2002)) occurs prior to atrophy in AD white matter (Chételat et al.,
29 2008), with the frontal cortex displaying loss of integrity comparatively later in the
30 disease than more posterior regions (Medina et al., 2006).

31

32 **Conclusions**

33

1 We have demonstrated that *post mortem* analysis of frontal cortex tissue from AD and
2 HC subjects displays a marked change in cortical grey matter iron distribution in this
3 degenerating region of the brain. Although this method is only possible using *post*
4 *mortem* tissue, we present important supporting evidence for existing MRI studies that
5 have focused on discerning white and grey matter iron distributions *in vivo* using a
6 highly sensitive and quantitative imaging approach. Results from this study highlight
7 a further need to understand the mechanisms by which iron may impart neurotoxicity
8 in AD.

9

10 **Acknowledgements**

11

12 The authors would like to thank Dr Ian Birchall and Dr Jeff Duyn for their helpful
13 advice, and Ms Fairlie Hilton of the Victorian Brain Bank Network for her assistance
14 with case notes. D.J.H. and P.A.D. are supported by funds from Australian Research
15 Council Linkage Project (LP120200081) in conjunction with ESI Ltd and Agilent
16 Technologies. D.J.H. and B.R.R. are additionally supported through Australian
17 Research Council Linkage Project (LP140100095) with Agilent Technologies. E.P.R.
18 is supported by the National Science Foundation Graduate Research Fellowship under
19 Grant No. DGE-1444316. P.J.C. is supported by funds from the National Health and
20 Medical Research Council (1005651 and 1061550). We gratefully acknowledge the
21 support of the Victorian Government's Operational Infrastructure Support Program
22 and the Victorian Brain Bank Network.

1 **References:**

- 2 Austin, C., Fryer, F., Lear, J., Bishop, D., Hare, D.J., Rawling, T., Doble, P., 2011.
3 Factors affecting internal standard selection for quantitative elemental bio-imaging of
4 soft tissues by LA-ICP-MS. *Journal of Analytical Atomic Spectrometry* 26, 1494-
5 1501.
- 6 Bartzokis, G., Cummings, J.L., Sultzer, D., Henderson, V.W., Nuechterlein, K.H.,
7 Mintz, J., 2003. White Matter Structural Integrity in Healthy Aging Adults and
8 Patients With Alzheimer Disease: A Magnetic Resonance Imaging Study. *Archives of*
9 *Neurology* 60, 393-398.
- 10 Bartzokis, G., Sultzer, D., Cummings, J., Holt, L.E., Hance, D.B., Henderson, V.W.,
11 Mintz, J., 2000. In vivo evaluation of brain iron in Alzheimer disease using magnetic
12 resonance imaging. *Archives of General Psychiatry* 57, 47-53.
- 13 Beilby, J.P., Prins, A.W., Swanson, N.R., 1999. Determination of hepatic iron
14 concentration in fresh and paraffin-embedded tissue. *Clinical Chemistry* 45, 573-574.
- 15 Belaidi, A.A., Bush, A.I., 2015. Iron neurochemistry in Alzheimer's disease and
16 Parkinson' disease: targets for therapeutics. *Journal of Neurochemistry*.
- 17 Bilgic, B., Pfefferbaum, A., Rohlfing, T., Sullivan, E.V., Adalsteinsson, E., 2012.
18 MRI estimates of brain iron concentration in normal aging using quantitative
19 susceptibility mapping. *NeuroImage* 59, 2625-2635.
- 20 Bishop, D.P., Clases, D., Fryer, F., Williams, E., Wilkins, S., Hare, D.J., Cole, N.,
21 Karst, U., Doble, P.A., 2015. Elemental bio-imaging using laser ablation-triple
22 quadrupole-ICP-MS. *Journal of Analytical Atomic Spectrometry*.
- 23 Blasko, I., Stampfer Kountchev, M., Robatscher, P., Veerhuis, R., Eikelenboom, P.,
24 Grubeck Loebenstein, B., 2004. How chronic inflammation can affect the brain and
25 support the development of Alzheimer's disease in old age: the role of microglia and
26 astrocytes. *Aging Cell* 3, 169-176.
- 27 Chen, L., Hambright, W.S., Na, R., Ran, Q., 2015. Ablation of the Ferroptosis
28 Inhibitor Glutathione Peroxidase 4 in Neurons Results in Rapid Motor Neuron
29 Degeneration and Paralysis. *Journal of Biological Chemistry* 290, 28097-28106.
- 30 Chételat, G., Desgranges, B., Landeau, B., Mézenge, F., Poline, J.B., de la Sayette,
31 V., Viader, F., Eustache, F., Baron, J.C., 2008. Direct voxel-based comparison
32 between grey matter hypometabolism and atrophy in Alzheimer's disease. *Brain* 131,
33 60-71.
- 34 Connor, J.R., Menzies, S.L., 1995. Cellular management of iron in the brain. *Journal*
35 *of the Neurological Sciences* 134 Suppl, 33-44.
- 36 Connor, J.R., Menzies, S.L., St Martin, S.M., Mufson, E.J., 1992a. A histochemical
37 study of iron, transferrin, and ferritin in Alzheimer's diseased brains. *Journal of*
38 *Neuroscience Research* 31, 75-83.

- 1 Connor, J.R., Snyder, B.S., Arosio, P., Loeffler, D.A., LeWitt, P., 1995. A
2 Quantitative Analysis of Isoferritins in Select Regions of Aged, Parkinsonian, and
3 Alzheimer's Diseased Brains. *Journal of Neurochemistry* 65, 717-724.
- 4 Connor, J.R., Snyder, B.S., Beard, J.L., Fine, R.E., Mufson, E.J., 1992b. Regional
5 distribution of iron and iron-regulatory proteins in the brain in aging and Alzheimer's
6 disease. *Journal of Neuroscience Research* 31, 327-335.
- 7 Crespo, A.C., Silva, B., Marques, L., Marcelino, E., Maruta, C., Costa, S., Timóteo,
8 A., Vilares, A., Couto, F.S., Faustino, P., Correia, A.P., Verdelho, A., Porto, G.,
9 Guerreiro, M., Herrero, A., Costa, C., de Mendonça, A., Costa, L., Martins, M., 2014.
10 Genetic and biochemical markers in patients with Alzheimer's disease support a
11 concerted systemic iron homeostasis dysregulation. *Neurobiology of Aging* 35, 777-
12 785.
- 13 Daugherty, A.M., Raz, N., 2015. Appraising the Role of Iron in Brain Aging and
14 Cognition: Promises and Limitations of MRI Methods. *Neuropsychology Review* 25,
15 272-287.
- 16 De Lucia, C., Rinchon, A., Olmos-Alonso, A., Riecken, K., Fehse, B., Boche, D.,
17 Perry, V.H., Gomez-Nicola, D., 2015. Microglia regulate hippocampal neurogenesis
18 during chronic neurodegeneration. *Brain, Behavior, and Immunity*.
- 19 Dixon, S.J., Lemberg, K.M., Lamprecht, M.R., Skouta, R., Zaitsev, E.M., Gleason,
20 C.E., Patel, D.N., Bauer, A.J., Cantley, A.M., Yang, W.S., Morrison III, B.,
21 Stockwell, B.R., 2012. Ferroptosis: An Iron-Dependent Form of Nonapoptotic Cell
22 Death. *Cell* 149, 1060-1072.
- 23 Drayer, B., Burger, P., Darwin, R., Riederer, S., Herfkens, R., Johnson, G.A., 1986.
24 MRI of brain iron. *American Journal of Roentgenology* 147, 103-110.
- 25 Duce, J.A., Tsatsanis, A., Cater, M.A., James, S.A., Robb, E., Wikke, K., Leong, S.L.,
26 Perez, K., Johanssen, T., Greenough, M.A., Cho, H.-H., Galatis, D., Moir, R.D.,
27 Masters, C.L., McLean, C., Tanzi, R.E., Cappai, R., Barnham, K.J., Ciccotosto, G.D.,
28 Rogers, J.T., Bush, A.I., 2010. Iron-Export Ferroxidase Activity of β -Amyloid
29 Precursor Protein Is Inhibited by Zinc in Alzheimer's Disease. *Cell* 142, 857-867.
- 30 Duyn, J.H., van Gelderen, P., Li, T.-Q., de Zwart, J.A., Koretsky, A.P., Fukunaga, M.,
31 2007. High-field MRI of brain cortical substructure based on signal phase.
32 *Proceedings of the National Academy of Sciences of the United States of America*
33 104, 11796-11801.
- 34 Fukunaga, M., Li, T.-Q., van Gelderen, P., de Zwart, J.A., Shmueli, K., Yao, B., Lee,
35 J., Maric, D., Aronova, M.A., Zhang, G., Leapman, R.D., Schenck, J.F., Merkle, H.,
36 Duyn, J.H., 2010. Layer-specific variation of iron content in cerebral cortex as a
37 source of MRI contrast. *Proceedings of the National Academy of Sciences of the*
38 *United States of America* 107, 3834-3839.
- 39 Gellein, K., Flaten, T.P., Erikson, K.M., Aschner, M., Syversen, T., 2007. Leaching of
40 Trace Elements from Biological Tissue by Formalin Fixation. *Biological Trace*
41 *Element Research* 121, 221-225.

- 1 Gomez-Nicola, D., Boche, D., 2015. Post-mortem analysis of neuroinflammatory
2 changes in human Alzheimer's disease. *Alzheimer's Research and Therapy* 7, 1.
- 3 Gunning-Dixon, F.M., Brickman, A.M., Cheng, J.C., Alexopoulos, G.S., 2009. Aging
4 of Cerebral White Matter: A Review of MRI Findings. *International Journal of*
5 *Geriatric Psychiatry* 24, 109-117.
- 6 Hackett, M.J., McQuillan, J.A., El-Assaad, F., Aitken, J.B., Levina, A., Cohen, D.D.,
7 Siegele, R., Carter, E.A., Grau, G.E., Hunt, N.H., Lay, P.A., 2011. Chemical
8 alterations to murine brain tissue induced by formalin fixation: implications for
9 biospectroscopic imaging and mapping studies of disease pathogenesis. *The Analyst*
10 136, 2941.
- 11 Hallgren, B., Sourander, P., 1958. The effect of age on the non-haemin iron in the
12 human brain. *Journal of Neurochemistry* 3, 41-51.
- 13 Hallgren, B., Sourander, P., 1960. The non-haemin iron in the cerebral cortex in
14 Alzheimer's disease. *Journal of Neurochemistry* 5, 307-310.
- 15 Hare, D.J., Austin, C., Doble, P., 2012a. Quantification strategies for elemental
16 imaging of biological samples using laser ablation-inductively coupled plasma-mass
17 spectrometry. *The Analyst* 137, 1527-1537.
- 18 Hare, D.J., Ayton, S., Bush, A., Lei, P., 2013a. A delicate balance: Iron metabolism
19 and diseases of the brain. *Frontiers in Aging Neuroscience* 5.
- 20 Hare, D.J., George, J.L., Bray, L., Volitakis, I., Vais, A., Ryan, T.M., Cherny, R.A.,
21 Bush, A.I., Masters, C.L., Adlard, P.A., 2014a. The effect of paraformaldehyde
22 fixation and sucrose cryoprotection on metal concentration in murine neurological
23 tissue. *Journal of Analytical Atomic Spectrometry*.
- 24 Hare, D.J., Gerlach, M., Riederer, P., 2012b. Considerations for measuring iron in
25 post-mortem tissue of Parkinson's disease patients. *Journal of Neural Transmission*
26 119, 1515-1521.
- 27 Hare, D.J., Lear, J., Bishop, D., Beavis, A., Doble, P.A., 2013b. Protocol for
28 production of matrix-matched brain tissue standards for imaging by laser ablation-
29 inductively coupled plasma-mass spectrometry. *Analytical Methods* 5, 1915-1921.
- 30 Hare, D.J., Lei, P., Ayton, S., Roberts, B.R., Grimm, R., George, J.L., Bishop, D.P.,
31 Beavis, A.D., Donovan, S.J., McColl, G., Volitakis, I., Masters, C.L., Adlard, P.A.,
32 Cherny, R.A., Bush, A.I., Finkelstein, D.I., Doble, P.A., 2014b. An iron-dopamine
33 index predicts risk of parkinsonian neurodegeneration in the substantia nigra pars
34 compacta. *Chemical Science* 5, 2160-2169.
- 35 Hare, D.J., New, E.J., de Jonge, M.D., McColl, G., 2015. Imaging metals in biology:
36 balancing sensitivity, selectivity and spatial resolution. *Chemical Society Reviews* 44,
37 5941-5958.
- 38 Hebbrecht, G., Maenhaut, W., Reuck, J.D., 1999. Brain trace elements and aging.
39 *Nuclear Instruments and Methods in Physics Research Section B: Beam Interactions*
40 *with Materials and Atoms* 150, 208-213.

- 1 James, S.A., Hare, D.J., Jenkins, N.L., de Jonge, M.D., Bush, A.I., McColl, G., 2016.
2 μ XANES: In vivo imaging of metal-protein coordination environments. *Scientific*
3 *Reports* 6, 20350.
- 4 Keep, R.F., Hua, Y., Xi, G., 2012. Brain Water Content: a Misunderstood
5 Measurement? *Translational Stroke Research* 3, 263-265.
- 6 Krebs, N., Langkammer, C., Goessler, W., Ropele, S., Fazekas, F., Yen, K., Scheurer,
7 E., 2014. Assessment of trace elements in human brain using inductively coupled
8 plasma mass spectrometry. - PubMed - NCBI. *Journal of Trace Elements in Medicine*
9 *and Biology* 28, 1-7.
- 10 Langkammer, C., Krebs, N., Goessler, W., Scheurer, E., Ebner, F., Yen, K., Fazekas,
11 F., Ropele, S., 2010. Quantitative MR Imaging of Brain Iron: A Postmortem
12 Validation Study. *Radiology* 257, 455-462.
- 13 Langkammer, C., Krebs, N., Goessler, W., Scheurer, E., Yen, K., Fazekas, F., Ropele,
14 S., 2012a. Susceptibility induced gray–white matter MRI contrast in the human brain.
15 *NeuroImage* 59, 1413-1419.
- 16 Langkammer, C., Ropele, S., Pirpamer, L., Fazekas, F., Schmidt, R., 2014. MRI for
17 iron mapping in Alzheimer's disease. *Neurodegenerative Diseases* 13, 189-191.
- 18 Langkammer, C., Schweser, F., Krebs, N., Deistung, A., Goessler, W., Scheurer, E.,
19 Sommer, K., Reishofer, G., Yen, K., Fazekas, F., Ropele, S., Reichenbach, J.R.,
20 2012b. Quantitative susceptibility mapping (QSM) as a means to measure brain iron?
21 A post mortem validation study. *NeuroImage* 62, 1593-1599.
- 22 Lear, J., Hare, D.J., Fryer, F., Adlard, P.A., Finkelstein, D.I., Doble, P.A., 2012. High-
23 resolution elemental bioimaging of Ca, Mn, Fe, Co, Cu, and Zn employing LA-ICP-
24 MS and hydrogen reaction gas. *Analytical Chemistry* 84, 6707-6714.
- 25 Leskovjan, A.C., Kretlow, A., Lanzirrotti, A., Barrea, R., Vogt, S., Miller, L.M., 2011.
26 Increased brain iron coincides with early plaque formation in a mouse model of
27 Alzheimer's disease. *NeuroImage* 55, 32-38.
- 28 Lodygensky, G.A., Marques, J.P., Maddage, R., Perroud, E., Sizonenko, S.V., Hüppi,
29 P.S., Gruetter, R., 2012. In vivo assessment of myelination by phase imaging at high
30 magnetic field. *NeuroImage* 59, 1979-1987.
- 31 Lovell, M.A., Robertson, J.D., Teesdale, W.J., Campbell, J.L., Markesbery, W.R.,
32 1998. Copper, iron and zinc in Alzheimer's disease senile plaques. *Journal of the*
33 *Neurological Sciences* 158, 47-52.
- 34 Medina, D., deToledo-Morrell, L., Urresta, F., Gabrieli, J.D.E., Moseley, M.,
35 Fleischman, D., Bennett, D.A., Leurgans, S., Turner, D.A., Stebbins, G.T., 2006.
36 White matter changes in mild cognitive impairment and AD: A diffusion tensor
37 imaging study. *Neurobiology of Aging* 27, 663-672.
- 38 Miliszkievicz, N., Walas, S., Tobiasz, A., 2015. Current approaches to calibration of
39 LA-ICP-MS analysis. *Journal of Analytical Atomic Spectrometry* 30, 327-338.

- 1 Miyajima, H., Takahashi, Y., Kono, S., Sugimoto, M., Suzuki, Y., Hishida, A.,
2 Sakamoto, M., Oucm, Y., 2002. Glucose and Oxygen Hypometabolism in
3 Aceruloplasminemia Brains. *Internal Medicine* 41, 186-190.
- 4 O'Reilly, J., Douglas, D., Braybrook, J., So, P.W., Vergucht, E., Garrevoet, J.,
5 Vekemans, B., Vincze, L., Goenaga-Infante, H., 2014. A novel calibration strategy for
6 the quantitative imaging of iron in biological tissues by LA-ICP-MS using matrix-
7 matched standards and internal standardisation. *Journal of Analytical Atomic*
8 *Spectrometry* 29.
- 9 Olmos-Alonso, A., Schettters, S.T.T., Sri, S., Askew, K., Mancuso, R., Vargas-
10 Caballero, M., Holscher, C., Perry, V.H., Gomez-Nicola, D., 2016. Pharmacological
11 targeting of CSF1R inhibits microglial proliferation and prevents the progression of
12 Alzheimer's-like pathology. *Brain*, awv379.
- 13 Ong, W.-Y., Farooqui, A.A., 2005. Iron, neuroinflammation, and Alzheimer's disease.
14 *Journal of Alzheimer's Disease* 8, 183-200.
- 15 Peters, D.G., Connor, J.R., Meadowcroft, M.D., 2015. The relationship between iron
16 dyshomeostasis and amyloidogenesis in Alzheimer's disease: Two sides of the same
17 coin. *Neurobiology of Disease* 81, 49-65.
- 18 Ramos, P., Santos, A., Pinto, N.R., Mendes, R., Magalhães, T., Almeida, A., 2014.
19 Iron levels in the human brain: a post-mortem study of anatomical region differences
20 and age-related changes. *Journal of Trace Elements in Medicine and Biology* 28, 13-
21 17.
- 22 Raven, E.P., Lu, P.H., Tishler, T.A., Heydari, P., Bartzokis, G., 2013. Increased iron
23 levels and decreased tissue integrity in hippocampus of Alzheimer's disease detected
24 in vivo with magnetic resonance imaging. *Journal of Alzheimer's Disease* 37, 127-
25 136.
- 26 Rembach, A., Hare, D.J., Lind, M., Fowler, C.J., Cherny, R.A., McLean, C., Bush,
27 A.I., Masters, C.L., Roberts, B.R., 2013. Decreased Copper in Alzheimer's Disease
28 Brain Is Predominantly in the Soluble Extractable Fraction. *International Journal of*
29 *Alzheimer's Disease* 2013, 1-7.
- 30 Riederer, P., Sofic, E., Rausch, W.-D., Schmidt, B., Reynolds, G.P., Jellinger, K.,
31 Youdim, M.B.H., 1989. Transition Metals, Ferritin, Glutathione, and Ascorbic Acid
32 in Parkinsonian Brains. *Journal of Neurochemistry* 52, 515-520.
- 33 Roberts, B.R., Ryan, T.M., Bush, A.I., Masters, C.L., Duce, J.A., 2011. The role of
34 metallobiology and amyloid- β peptides in Alzheimer's disease. *Journal of*
35 *Neurochemistry* 120, 149-166.
- 36 Rossi, M., Ruottinen, H., Soimakallio, S., Elovaara, I., Dastidar, P., 2013. Clinical
37 MRI for iron detection in Parkinson's disease. *Clinical Imaging* 37, 631-636.
- 38 Schindelin, J., Arganda-Carreras, I., Frise, E., Kaynig, V., Longair, M., Pietzsch, T.,
39 Preibisch, S., Rueden, C., Saalfeld, S., Schmid, B., Tinevez, J.-Y., White, D.J.,
40 Hartenstein, V., Eliceiri, K., Tomancak, P., Cardona, A., 2012. Fiji: an open-source
41 platform for biological-image analysis. *Nature Methods* 9, 676-682.

- 1 Schipper, H.M., 2004. Brain iron deposition and the free radical-mitochondrial theory
2 of ageing. *Ageing Research Reviews* 3, 265-301.
- 3 Schrag, M., Dickson, A., Jiffry, A., Kirsch, D., Vinters, H.V., Kirsch, W., 2010. The
4 effect of formalin fixation on the levels of brain transition metals in archived samples.
5 *BioMetals* 23, 1123-1127.
- 6 Schrag, M., Mueller, C., Oyoyo, U., Smith, M.A., Kirsch, W.M., 2011. Iron, zinc and
7 copper in the Alzheimer's disease brain: A quantitative meta-analysis. Some insight
8 on the influence of citation bias on scientific opinion. *Progress in Neurobiology* 94,
9 296-306.
- 10 Snedecor, G., Cochran, W., 1986. *Statistical Methods*, 8th ed. Iowa State University
11 Press.
- 12 Stüber, C., Morawski, M., Schäfer, A., Labadie, C., Wähnert, M., Leuze, C.,
13 Streicher, M., Barapatre, N., Reimann, K., Geyer, S., Spemann, D., Turner, R., 2014.
14 Myelin and iron concentration in the human brain: A quantitative study of MRI
15 contrast. *NeuroImage* 93, 95-106.
- 16 van Duijn, S., Nabuurs, R.J.A., van Duinen, S.G., Natte, R., 2013. Comparison of
17 Histological Techniques to Visualize Iron in Paraffin-embedded Brain Tissue of
18 Patients with Alzheimer's Disease. *Journal of Histochemistry and Cytochemistry* 61,
19 785-792.
- 20 Ward, R.R., Zucca, F.A., Duyn, J.H., Crichton, R.R., Zecca, L., 2014. The role of iron
21 in brain ageing and neurodegenerativedisorders. *Lancet Neurology* 13, 1045-1060.
- 22 Wong, B.X., Tsatsanis, A., Lim, L.Q., Adlard, P.A., Bush, A.I., Duce, J.A., 2014. β -
23 Amyloid Precursor Protein Does Not Possess Ferroxidase Activity but Does Stabilize
24 the Cell Surface Ferrous Iron Exporter Ferroportin. *PLoS One* 9, e114174.
- 25 Yeatman, J.D., Wandell, B.A., Mezer, A.A., 2014. Lifespan maturation and
26 degeneration of human brain white matter. *Nature Communications* 5, 4932.
- 27 Zecca, L., Pietra, R., Goj, C., Mecacci, C., Radice, D., Sabbioni, E., 1994. Iron and
28 other metals in neuromelanin, substantia nigra, and putamen of human brain. *Journal*
29 *of Neurochemistry* 62, 1097-1101.
- 30 Zecca, L., Stroppolo, A., Gatti, A., Tampellini, D., Toscani, M., Gallorini, M.,
31 Giaveri, G., Arosio, P., Santambrogio, P., Fariello, R.G., 2004. The role of iron and
32 copper molecules in the neuronal vulnerability of locus coeruleus and substantia nigra
33 during aging. *Proceedings of the National Academy of Sciences of the United States*
34 *of America* 101, 9843.
- 35 Zeineh, M.M., Chen, Y., Kitzler, H.H., Hammond, R., Vogel, H., Rutt, B.K., 2015.
36 Activated iron-containing microglia in the human hippocampus identified by
37 magnetic resonance imaging in Alzheimer disease. *Neurobiology of Aging* 36, 2483-
38 2500.

- 1 Zhu, W.-z., Zhong, W.-d., Wang, W., Zhan, C.-j., Wang, C.-y., Qi, J.-p., Wang, J.-z.,
- 2 Lei, T., 2009. Quantitative MR Phase-corrected Imaging to Investigate Increased
- 3 Brain Iron Deposition of Patients with Alzheimer Disease. *Radiology* 253, 497-504.
- 4

10. Supplementary Material

[Click here to download 10. Supplementary Material: Iron in AD SI.pdf](#)



Minerva Access is the Institutional Repository of The University of Melbourne

Author/s:

Hare, DJ; Raven, EP; Roberts, BR; Bogeski, M; Portbury, SD; McLean, CA; Masters, CL; Connor, JR; Bush, AI; Crouch, PJ; Doble, PA

Title:

Laser ablation-inductively coupled plasma-mass spectrometry imaging of white and gray matter iron distribution in Alzheimer's disease frontal cortex

Date:

2016-08-15

Citation:

Hare, D. J., Raven, E. P., Roberts, B. R., Bogeski, M., Portbury, S. D., McLean, C. A., Masters, C. L., Connor, J. R., Bush, A. I., Crouch, P. J. & Doble, P. A. (2016). Laser ablation-inductively coupled plasma-mass spectrometry imaging of white and gray matter iron distribution in Alzheimer's disease frontal cortex. *NEUROIMAGE*, 137, pp.124-131. <https://doi.org/10.1016/j.neuroimage.2016.05.057>.

Persistent Link:

<http://hdl.handle.net/11343/191291>

File Description:

Submitted Version